

Cross bispectra and trispectra of the non-linear integrated Sachs-Wolfe effect and the tracer galaxy density field

Gero Jürgens^{*1} and Björn Malte Schäfer²

¹*Institut für theoretische Astrophysik, Zentrum für Astronomie, Universität Heidelberg, Philosophenweg 12, 69120 Heidelberg, Germany*

²*Astronomisches Recheninstitut, Zentrum für Astronomie, Universität Heidelberg, Mönchhofstraße 12, 69120 Heidelberg, Germany*

24 August 2021

ABSTRACT

In order to investigate possibilities to measure non-Gaussian signatures of the non-linear iSW effect, we study in this work the family of mixed bispectra $\langle \tau^q \gamma^{3-q} \rangle$ and trispectra $\langle \tau^q \gamma^{4-q} \rangle$ between the integrated Sachs-Wolfe (iSW) temperature perturbation τ and the galaxy overdensity γ . We use standard Eulerian perturbation theory restricted to tree level expansion for predicting the cosmic matter field. As expected, the spectra are found to decrease in amplitude with increasing q . The transition scale between linear domination and the scales, on which non-linearities take over, moves to larger scales with increasing number of included iSW source fields q . We derive the cumulative signal-to-noise ratios for a combination of *Planck* CMB data and the galaxy sample of a *Euclid*-like survey. Including scales down to $\ell_{\max} = 1000$ we find sobering values of $\sigma \approx 0.83$ for the mixed bispectrum and $\sigma \approx 0.19$ in case of the trispectrum for $q = 1$. For higher values of q the polyspectra $\langle \tau^2 \gamma \rangle$ and $\langle \tau^3 \gamma \rangle$ are found to be far below the detection limit.

Key words: cosmology: large-scale structure, integrated Sachs-Wolfe effect, methods: analytical

1 INTRODUCTION

The integrated Sachs-Wolfe (iSW) effect is one of the secondary anisotropies of the cosmic microwave background (CMB). Time-evolving gravitational potentials in the large-scale structure generate temperature fluctuations in the CMB (Sachs & Wolfe 1967). The linear part of this effect is a valuable tool for investigating dark energy and non-standard cosmologies since it is sensitive to fluids with non-zero equation of state (Crittenden & Turok 1996). For this reason its detection is of particular relevance for cosmology and the nature of gravity (Lue et al. 2004; Zhang 2006) even though its signal strength is very low.

The linear iSW effect has been measured in such cross-correlation studies (Boughn et al. 1998; Boughn & Crittenden 2004; Vielva et al. 2006; McEwen et al. 2007; Giannantonio et al. 2008). There are, however, doubts on detection claims formulated by Hernández-Monteagudo (2010) and López-Corredoira et al. (2010), who point out that the iSW-signal seems to be too weak on low multipoles below $\ell \sim 10$, and that field-to-field fluctuations and sampling errors can be important. These facts may correct the detection significance to-date to a number of less than two.

While the linear iSW signal is a large scale effect and becomes negligible at angular wave numbers above $\ell \sim 100$, non-linear evolution of the gravitational potential and leaves signatures on much smaller scales, also called Rees-Sciama effect (Rees & Sciama

1968) and surpasses the linear iSW-effect on these scales. The possible signatures of this effect in angular cross spectrum have been thoroughly studied analytically (Martinez-Gonzalez et al. 1994; Sanz et al. 1996; Seljak 1996; Schäfer & Bartelmann 2006). The effect increases the total iSW signal by roughly two orders of magnitude at angular scales around $\ell \sim 1000$ (Cooray 2002), before gravitational lensing and kinetic Sunyaev-Zel'dovich effect become dominant at even smaller scales. However, comparisons of theoretical studies with numerical simulations showed the Rees-Sciama to be negligible in comparison with primary anisotropies on angular scales larger than $\theta > 1'$ (Tuluie & Laguna 1995; Seljak 1996). Also from cross-correlations of the CMB with weak lensing surveys only a detection significance of $\sim 1.5\sigma$ from *Planck*+LSST is expected (Nishizawa et al. 2008).

One option to obtain direct signatures of non-Gaussianities is the investigation of higher order connected correlators (Schäfer 2008). In this work we aim to formulate a perturbative approach of the mixed iSW-galaxy polyspectra, concentrating on the tree-level bispectra and trispectra in flat sky approximation. The unequal rate of linear and non-linear evolution at different scales will lead to interesting sign changes in the spectra, which will also be apparent in the non-trivial time evolution of the different source field contributions. In addition, we will study the signal-to-noise spectra for measurements expected from *Planck* CMB data in cross-correlation with observations from a *Euclid*-like survey assuming unbiased measurements with Gaussian noise contributions. We revisit a previous estimate of the observability of the iSW-bispectrum (Schäfer

* gero.juergens@stud.uni-heidelberg.de

2008) correcting an error in the expression for the spectrum of the gravitational potential and because of the significantly improved signal-to-noise computation, which uses an adaptive Monte-Carlo integration scheme (Hahn 2005) instead of a binned summation over the multipoles.

The article has the following structure: In Section 2 we will lay out the theoretical framework for linear and non-linear structure formation (Section 2.3 and Section 2.4), as well as for the theory of higher order correlators of the density field in Section 2.5. Furthermore, the main fields of interest, the galaxy number distribution (Section 2.6) and the iSW-effect (Section 2.6) are introduced. The mixed bispectra and trispectra are discussed in Section 3, with specific studies of their weighting functions (Section 3.4) and their time evolution (Section 3.5). In Section 4 we present the relevant noise sources (Section 4.1), the resulting covariances (Section 4.2) of the polyspectra and finally derive their signal-to-noise ratios (Section 4.3). Our results are summarized and discussed in Section 5.

The reference cosmological model used is a spatially flat Λ CDM cosmology with Gaussian adiabatic initial perturbations in the cold dark matter density field. The specific parameter choices are $\Omega_m = 0.25$, $n_s = 1$, $\sigma_8 = 0.8$, $\Omega_b = 0.04$ and $H_0 = 100 h$ km/s/Mpc, with $h = 0.72$.

2 FOUNDATIONS

2.1 Dark energy cosmologies

In spatially flat dark energy cosmologies with the matter density parameter Ω_m , the Hubble function $H(a) = d \ln a / dt$ is given by

$$\frac{H^2(a)}{H_0^2} = \Omega_m a^{-3} + (1 - \Omega_m) a^{-3(1+w)}, \quad (1)$$

with a constant dark energy equation of state parameter w . The value $w \equiv -1$ corresponds to the cosmological constant Λ . The relation between comoving distance χ and scale factor a is given by

$$\chi = c \int_a^1 da \frac{1}{a^2 H(a)}, \quad (2)$$

in units of the Hubble distance $\chi_H = c/H_0$.

2.2 CDM power spectrum

The CDM density power spectrum $P(k)$ describes the fluctuation amplitude of the Gaussian homogeneous density field $\delta(\mathbf{k})$, $\langle \delta(\mathbf{k}) \delta^*(\mathbf{k}') \rangle = (2\pi)^3 \delta_D(\mathbf{k} - \mathbf{k}') P(k)$, and the power spectrum of linear evolving density fields $\delta_L(\mathbf{k})$ is given by the ansatz

$$P_L(k) \propto k^{ns} T^2(k), \quad (3)$$

with the transfer function $T(k)$. In low- Ω_m cosmologies $T(k)$ is approximated with the fit proposed by Bardeen et al. (1986),

$$T(q) = \frac{\ln(1 + 2.34 q)}{2.34 q} \times \left[1 + 3.89 q + (16.1 q)^2 + (5.46 q)^3 + (6.71 q)^4 \right]^{-1/4} \quad (4)$$

where the wave number $k = q\Gamma$ is rescaled with the shape parameter Γ (Sugiyama 1995) which assumes corrections due to the baryon density Ω_b ,

$$\Gamma = \Omega_m h \exp \left[-\Omega_b \left(1 + \frac{\sqrt{2h}}{\Omega_m} \right) \right]. \quad (5)$$

The spectrum $P(k)$ is normalized to the variance σ_8 on the scale $R = 8$ Mpc/ h ,

$$\sigma_R^2 = \frac{1}{2\pi^2} \int dk k^2 P(k) W^2(kR) \quad (6)$$

with a Fourier transformed spherical top hat filter function, $W(x) = 3j_1(x)/x$. $j_\ell(x)$ is the spherical Bessel function of the first kind of order ℓ (Abramowitz & Stegun 1972).

2.3 Linear structure growth

The linear homogeneous growth of the relative density perturbation field $\delta_L(\mathbf{x}, a)$ is described by the growth function $D_+(a)$

$$\delta_L(\mathbf{k}, a) = D_+(a) \delta_L(\mathbf{k}, a = 1), \quad (7)$$

which is the solution to the growth equation (Turner & White 1997; Wang & Steinhardt 1998; Linder & Jenkins 2003),

$$\frac{d^2}{da^2} D_+(a) + \frac{1}{a} \left(3 + \frac{d \ln H}{d \ln a} \right) \frac{d}{da} D_+(a) = \frac{3}{2a^2} \Omega_m(a) D_+(a). \quad (8)$$

The growth equation can be obtained by combining the linearized structure formation equations consisting of Poisson equation, Euler equation and continuity equation.

Considering the special case of flat SCDM cosmologies, where $\Omega_m \equiv 1$, the Hubble function scales like $H = H_0 a^{-3/2}$. The growing mode solution then gives the very simple growth function $D_+(a) = a$, which is even in more complex cosmologies a good approximation during the matter domination era.

2.4 Non-linear structure formation

In order to describe non-Gaussianities in the density source field generated by non-linear evolution a theoretical approximation is required.

We employ non-linear solutions to the density field from standard Eulerian perturbation theory (Sahni & Coles 1995; Bernardeau et al. 2002). One expands the density contrast $\delta(\mathbf{k}, a)$ in n -th order perturbative contributions $\delta^{(n)}(\mathbf{k}, a)$, which can be written in terms of the perturbation theory kernels $F^{(n)}(\mathbf{k}_1, \dots, \mathbf{k}_n)$ and the initial linear fields $\delta^{(1)}(\mathbf{k}) = \delta_L(\mathbf{k}, a = 1)$:

$$\delta(\mathbf{k}, a) = \sum_{n=1}^{\infty} D_+^n \delta^{(n)}(\mathbf{k}) \quad (9)$$

$$\delta^{(n)}(\mathbf{k}) = \int d^3 q_1 \dots \int d^3 q_n \delta_D(\mathbf{k} - \mathbf{q}_{1\dots n}) \times F^{(n)}(\mathbf{q}_1, \dots, \mathbf{q}_n) \delta^{(1)}(\mathbf{q}_1) \dots \delta^{(1)}(\mathbf{q}_n) \quad (10)$$

with $\mathbf{q}_{1\dots n} = \mathbf{q}_1 + \dots + \mathbf{q}_n$. By inserting eqs. (9-10) into the evolution equations one finds recursion relations for the kernels $F^{(n)}(\mathbf{q}_1, \dots, \mathbf{q}_n)$ by combinatorics (Goroff et al. 1986; Jain & Bertschinger 1994). The explicit symmetrized expressions for the second order perturbation theory kernels take a very simple and intuitive form:

$$F^{(2)}(\mathbf{k}_1, \mathbf{k}_2) = \frac{5}{7} + \frac{1}{2} \frac{\mathbf{k}_1 \cdot \mathbf{k}_2}{k_1 k_2} \left(\frac{k_1}{k_2} + \frac{k_2}{k_1} \right) + \frac{2}{7} \frac{(\mathbf{k}_1 \cdot \mathbf{k}_2)^2}{k_1^2 k_2^2} \quad (11)$$

$$G^{(2)}(\mathbf{k}_1, \mathbf{k}_2) = \frac{3}{7} + \frac{1}{2} \frac{\mathbf{k}_1 \cdot \mathbf{k}_2}{k_1 k_2} \left(\frac{k_1}{k_2} + \frac{k_2}{k_1} \right) + \frac{4}{7} \frac{(\mathbf{k}_1 \cdot \mathbf{k}_2)^2}{k_1^2 k_2^2}, \quad (12)$$

where $F^{(1)} = G^{(1)} = 1$. One can see that mode-coupling to second order reaches its maximum when the contributing modes \mathbf{k}_1 and \mathbf{k}_2 are aligned, whereas the kernel vanishes for anti-parallel modes.

When in eqn. (10) n different modes $\mathbf{q}_1 \dots \mathbf{q}_n$ contribute to a mode \mathbf{k} , wave number conservation holds, enforced by the δ_D -distribution: $\mathbf{k} = \mathbf{q}_1 + \dots + \mathbf{q}_n$.

2.5 The n -point functions in perturbation theory

For an analytic expression of the perturbation theory n -point function one has to expand the fields in the correlator. Due to the assumed Gaussianity of the initial field $\delta^{(1)}$ the correlators with an even number of fields $\delta^{(1)}$ will later simplify to products of initial two-point functions $P_L(k)$, while all uneven contributions vanish:

$$\langle \delta_1 \dots \delta_n \rangle = \left\langle \sum_{i_1} D_+^{i_1} \delta_1^{(i_1)} \dots \sum_{i_n} D_+^{i_n} \delta_n^{(i_n)} \right\rangle. \quad (13)$$

For simplicity we use in this subsection the notation $\delta_n \equiv \delta(\mathbf{k}_n)$. Simple truncation of the expansion in eqn. (9) would lead to an inconsistent inclusion of powers of the linear power spectrum $P_L(k)$. It is more sensitive to take into account all terms up to a certain power m in the linear power spectrum, which is equivalent to including terms with initial fields up to powers $2m$.

In this work we exclusively use tree-level perturbation theory, i.e. no perturbative terms with wave number integrations are taken into account. Following this path, the density bispectrum $B_\delta^{\mathbf{k}_1, \mathbf{k}_2, \mathbf{k}_3}$ can be written as

$$B_\delta^{\mathbf{k}_1, \mathbf{k}_2, \mathbf{k}_3} = 2 F^{(2)}(\mathbf{k}_1, \mathbf{k}_2) P_L(k_1) P_L(k_2) + \text{cycl. } \{1, 2, 3\}. \quad (14)$$

The non-Gaussian part of the 4-point function is the trispectrum $T_\delta^{\mathbf{k}_1, \mathbf{k}_2, \mathbf{k}_3, \mathbf{k}_4}$. It is convenient to split its tree-level expression up into two parts. The first contribution originates from second order perturbation theory. In this case, two of the fields in the correlator have been expanded to second order. The expressions in terms of the initial power spectra and the second order kernels are of the type

$$\begin{aligned} t^{(2)}((\mathbf{k}_1, \mathbf{k}_2), (\mathbf{k}_3, \mathbf{k}_4)) &= 4 D_+^6 P_L(k_3) P_L(k_4) \times \\ &\left(F^{(2)}(\mathbf{k}_{13}, -\mathbf{k}_3) F^{(2)}(\mathbf{k}_{24}, -\mathbf{k}_4) P_L(k_{13}) \right. \\ &\left. + F^{(2)}(\mathbf{k}_{14}, -\mathbf{k}_4) F^{(2)}(\mathbf{k}_{23}, -\mathbf{k}_3) P_L(k_{14}) \right). \end{aligned} \quad (15)$$

The second contribution is due to third order perturbation theory. Here, one field is expanded to third order while the other three remain at linear order. For this reason only one perturbation kernel appears in the expression for this type of contributions

$$t^{(3)}(\mathbf{k}_1, \mathbf{k}_2, \mathbf{k}_3, \mathbf{k}_4) = 6 D_+^6 F^{(3)}(\mathbf{k}_1, \mathbf{k}_2, \mathbf{k}_3) P_L(k_1) P_L(k_2) P_L(k_3). \quad (16)$$

With these two functions the connected perturbation theory four-point function up to third order in the linear power spectrum $P_L(k)$ can be expressed by the following two tree-level contributions

$$\begin{aligned} T_\delta^{\mathbf{k}_1, \mathbf{k}_2, \mathbf{k}_3, \mathbf{k}_4} &= t^{(2)}((\mathbf{k}_1, \mathbf{k}_2), (\mathbf{k}_3, \mathbf{k}_4)) + \text{all pairs } \in \{1, 2, 3, 4\} \\ &+ t^{(3)}(\mathbf{k}_1, \mathbf{k}_2, \mathbf{k}_3, \mathbf{k}_4) + \text{cycl. } \{1, 2, 3, 4\}. \end{aligned} \quad (17)$$

The second order and the third order contributions of T_δ , however, have the same time dependence D_+^6 . We will see, that this is not longer the case for mixed trispectra.

2.6 Galaxy distribution

Galaxies form when strong peaks in the density field decouple from the Hubble expansion due to self-gravity. These so called protohalos undergo an elliptical collapse (Mo et al. 1997; Sheth et al. 2001).

In contrary to the pressure-less dark matter component the

baryons inside a dark matter halo can loose energy via radiative cooling and form stars. Because of the more complex behavior of baryons, the relation between the fractional perturbation $\Delta n / \langle n \rangle$ in the mean number density of galaxies $\langle n \rangle$ and the dark matter overdensity $\delta = \Delta \rho / \rho$ is not yet understood. In a very simple way, however, the linear relation between the two entities,

$$\frac{\Delta n}{\langle n \rangle} = b \frac{\Delta \rho}{\rho}, \quad (18)$$

is a good approximation in most cases and was proposed by Bardeen et al. (1986). The bias parameter b can generally depend on a number of variables but for simplicity we set the galaxy bias to unity throughout this paper, $b \equiv 1$. An established parametrization of the redshift distribution $n(z) dz$ of galaxies is

$$n(z) dz = n_0 \left(\frac{z}{z_0} \right)^2 \exp \left[- \left(\frac{z}{z_0} \right)^\beta \right] dz \quad \text{with} \quad \frac{1}{n_0} = \frac{z_0}{\beta} \Gamma \left(\frac{3}{\beta} \right) \quad (19)$$

which was introduced by Smail et al. (1995) and will also be used in this work. The parameter z_0 is related to the median redshift of the galaxy sample $z_{\text{med}} = 1.406 z_0$ if $\beta = 3/2$. For *Euclid* the median redshift is $z_{\text{med}} = 0.9$. Finally, the Γ -function (Abramowitz & Stegun 1972) determines the normalization parameter n_0 .

2.7 ISW-effect

Due to its expansion our universe had cooled down sufficiently to allow the formation of hydrogen atoms at a redshift of $z \approx 1089$ (Spergel et al. 2003). Fluctuations in the gravitational potential imposed a shift in the decoupled photons which were emitted in the (re)combination process (Sachs-Wolfe effect). This primary anisotropy can be observed in the cosmic microwave background (CMB) in form of temperature fluctuations $\Delta T / T_{\text{CMB}} \approx 10^{-5}$ on large scales around its mean temperature $T_{\text{CMB}} = 2.726$ K (Fixsen 2009).

Besides this, photons are subjected to several other effects on their way to us, which lead to secondary anisotropies (reviewed by Aghanim et al. 2008), of which only the most important ones are mentioned here: Gravitational lensing (Hu 2000), Compton-collisions with free cluster electrons (Sunyaev-Zeldovich effect, Zeldovich & Sunyaev 1980) and with electrons in uncollapsed structures (Ostriker-Vishniac effect, Ostriker & Vishniac 1986) and gravitational coupling to linear (Sachs & Wolfe 1967, integrated Sachs-Wolfe effect,) and non-linear time-evolving potential wells (Rees & Sciama 1968). Heuristically, the latter two effects originate from an unbalance between the photon's blue-shift when entering a time varying potential well and the red-shift experienced at the exit.

Assuming a completely transparent space, i.e. vanishing optical depth due to Compton scattering, the temperature fluctuations $\tau(\hat{\theta})$ generated by the iSW-effect can be expressed by the line of sight integral (Sachs & Wolfe 1967)

$$\tau(\theta) \equiv \frac{\Delta T_{\text{iSW}}}{T_{\text{CMB}}} = \frac{2}{c^3} \int_0^{\chi_H} d\chi a^2 H(a) \frac{\partial}{\partial a} \Phi(\theta_\chi, \chi), \quad (20)$$

reaching out to the limit of Newtonian gravity. Using the Poisson equation we can write this integral in terms of the dimensionless potential $\phi = \Delta^{-1} \delta / \chi_H^2$ of the density field $\delta(\theta_\chi, \chi)$. The n -th perturbative order of the iSW temperature fluctuation $\tau = \tau^{(1)} + \tau^{(2)} + \dots$ can now be written as

$$\tau^{(n)}(\theta) = \frac{3 \Omega_m}{c} \int_0^{\chi_H} d\chi a^2 H(a) \frac{\Delta^{-1}}{\chi_H^2} \left(\frac{d}{da} \frac{D_+^{(n)}}{a} \right) \delta(\theta_\chi, \chi). \quad (21)$$

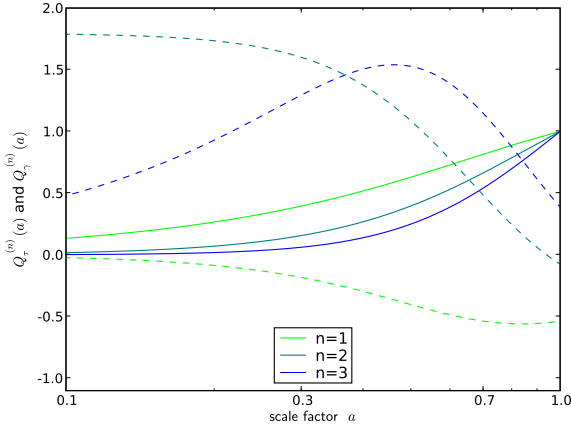


Figure 1. Time evolution functions $Q_\gamma^{(n)}(a)$ (solid lines) and $Q_\tau^{(n)}(a)$ (dashed lines) as a function of the scale factor a for different perturbative orders $n = 1, 2, 3$.

The linear effect ($n = 1$) vanishes identically in matter dominated universes $\Omega_m = 1$, since then D_+/a is a constant. Therefore, a non-zero iSW-signal will be an indicator of a cosmological fluid with $w \neq 0$. After the radiation dominated era it will thus be a valuable tool for investigating dark energy cosmologies. The non-linear contributions ($n \geq 2$) are now sourced by time derivatives of the higher perturbative orders of the gravitational potential. Therefore, the Rees-Sciama effect is also present in SCDM-cosmology.

In order to identify the sources of the effect it is sensible to investigate the cross correlation of the iSW amplitude with the line of sight projected relative galaxy over-density $\gamma = \gamma^{(1)} + \gamma^{(2)} + \dots$

$$\gamma^{(n)}(\boldsymbol{\theta}) = b \int_0^{\chi_H} d\chi n(z) \frac{dz}{d\chi} D_+^n \delta(\boldsymbol{\theta}\chi, \chi). \quad (22)$$

Since we are interested in rather small scales, where non-linear effects appear, one can approximate the sphere locally as being plane and perform a Fourier transform

$$\gamma(\boldsymbol{\ell}) = \int d^2\theta \gamma(\boldsymbol{\theta}) e^{-i(\boldsymbol{\ell} \cdot \boldsymbol{\theta})}. \quad (23)$$

The observable τ can be transformed in analogous way. For later notational convenience we define the two weighting functions

$$\begin{aligned} W_\gamma(\chi) &= b n(z) \frac{dz}{d\chi} \\ W_\tau(\chi) &= 3 \Omega_m a^2 \frac{H}{c} \end{aligned} \quad (24)$$

and the time evolution functions to n -th order

$$\begin{aligned} Q_\gamma^{(n)}(a) &= D_+^n \\ Q_\tau^{(n)}(a) &= \frac{d}{da} \left(\frac{D_+^n}{a} \right). \end{aligned} \quad (25)$$

In Fig. 1 the time evolution functions $Q_\gamma^{(n)}(a)$ and $Q_\tau^{(n)}(a)$ are depicted in dependence on the scale factor a . It is particularly interesting to observe the different signs. While the galaxy spectra are always positive, the iSW contributions change their signs with perturbative order. As we will later observe, also the signs of n -point functions will change consequently in the transition from large scales, where the linear theory is valid, to small scales, where non-linearities start to dominate. For the cross-bispectrum, this effect has already been studied (Nishizawa et al. 2008).

3 MIXED BISPECTRA AND TRISPECTRA

3.1 The density polyspectra

Regardless of the existence of initial non-Gaussianities in the density field $\delta(\mathbf{k})$, non-linear structure formation leads to non-vanishing three-point and higher order correlators due to quadratic terms in the continuity and Euler equation. Since a Gaussian field can uniquely be represented by its two-point correlator $\xi(r) = \langle \delta(\mathbf{x})\delta(\mathbf{x} + \mathbf{r}) \rangle$, multi-point correlators represent a convenient measure of evolving non-Gaussianities. The Fourier transforms of these 2-point and 3-point correlators are the bispectrum $B_\delta^{\mathbf{k}_1, \mathbf{k}_2, \mathbf{k}_3}$ and the trispectrum $T_\delta^{\mathbf{k}_1, \mathbf{k}_2, \mathbf{k}_3, \mathbf{k}_4}$

$$\begin{aligned} \langle \delta(\mathbf{k}_1)\delta(\mathbf{k}_2)\delta(\mathbf{k}_3) \rangle &= (2\pi)^3 \delta_D(\mathbf{k}_{1\dots 3}) B_\delta^{\mathbf{k}_1, \mathbf{k}_2, \mathbf{k}_3} \\ \langle \delta(\mathbf{k}_1)\delta(\mathbf{k}_2)\delta(\mathbf{k}_3)\delta(\mathbf{k}_4) \rangle_c &= (2\pi)^3 \delta_D(\mathbf{k}_{1\dots 4}) T_\delta^{\mathbf{k}_1, \mathbf{k}_2, \mathbf{k}_3, \mathbf{k}_4}, \end{aligned} \quad (26)$$

where the Dirac δ_D -function is a result of homogeneity.

3.2 Limber Projection

In the flat sky approximation one can use a simplified Limber projection (Limber 1953) to relate the 3-dimensional source spectra $B_\delta^{\mathbf{k}_1, \mathbf{k}_2, \mathbf{k}_3}$ and $T_\delta^{\mathbf{k}_1, \mathbf{k}_2, \mathbf{k}_3, \mathbf{k}_4}$ to the angular spectra $B_\gamma^{\ell_1, \ell_2, \ell_3}$ and $T_\gamma^{\ell_1, \ell_2, \ell_3, \ell_4}$.

$$\begin{aligned} B_\gamma^{\ell_1, \ell_2, \ell_3} &= \int_0^{\chi_H} d\chi \frac{1}{\chi^4} W_\gamma^3(\chi) D_+^4(a) B_\delta^{\mathbf{k}_1, \mathbf{k}_2, \mathbf{k}_3} \\ T_\gamma^{\ell_1, \ell_2, \ell_3, \ell_4} &= \int_0^{\chi_H} d\chi \frac{1}{\chi^6} W_\gamma^4(\chi) D_+^6(a) T_\delta^{\mathbf{k}_1, \mathbf{k}_2, \mathbf{k}_3, \mathbf{k}_4}. \end{aligned} \quad (27)$$

Then, equivalent formulae as in eqn. (26) apply to these angular polyspectra, which are then related to the projected density field $\gamma(\boldsymbol{\ell})$ with two-dimensional angular wave vectors $\boldsymbol{\ell}_i$:

$$\begin{aligned} \langle \gamma(\boldsymbol{\ell}_1)\gamma(\boldsymbol{\ell}_2)\gamma(\boldsymbol{\ell}_3) \rangle &= (2\pi)^3 \delta_D(\boldsymbol{\ell}_{1\dots 3}) B_\gamma^{\ell_1, \ell_2, \ell_3} \\ \langle \gamma(\boldsymbol{\ell}_1)\gamma(\boldsymbol{\ell}_2)\gamma(\boldsymbol{\ell}_3)\gamma(\boldsymbol{\ell}_4) \rangle &= (2\pi)^3 \delta_D(\boldsymbol{\ell}_{1\dots 4}) T_\gamma^{\ell_1, \ell_2, \ell_3, \ell_4}, \end{aligned} \quad (28)$$

where the fields on the sphere with angular directions \mathbf{n}_i are simply decomposed into Fourier harmonics instead of spherical harmonics

$$\begin{aligned} \langle \gamma(\mathbf{n}_1)\dots\gamma(\mathbf{n}_n) \rangle &= \int \frac{d^2\ell_1}{(2\pi)^2} \dots \int \frac{d^2\ell_n}{(2\pi)^2} \\ &\cdot \langle \gamma(\boldsymbol{\ell}_1)\dots\gamma(\boldsymbol{\ell}_n) \rangle e^{i\ell_1 \cdot \mathbf{n}_1} \dots e^{i\ell_n \cdot \mathbf{n}_n}. \end{aligned} \quad (29)$$

Since the region on a sphere around a certain point can for small angles be approximated by the tangential plane, this is a good approximation for high ℓ -values. It can generally be transformed to the full sky representation with Wigner 3j-symbols (Hu 2001).

3.3 Mixed iSW-galaxy polyspectra

An equivalent procedure of definitions as in the previous subsection can be applied to the iSW-fields $\tau(\boldsymbol{\ell})$. However, due to the uncorrelated noise sources in the iSW and galaxy fields mixed spectra are of predominant interest to us. If there exists a chance to securely measure the iSW signal it will only work via its cross-correlation to the projected galaxy density field $\gamma(\boldsymbol{\ell})$ in the cross power spectrum and higher order correlators.

To allow a compact definition of the mixed spectra we introduce a doublet field $\varphi_i(\boldsymbol{\ell})$

$$\begin{pmatrix} \varphi_0(\boldsymbol{\ell}) \\ \varphi_1(\boldsymbol{\ell}) \end{pmatrix} = \begin{pmatrix} \gamma(\boldsymbol{\ell}) \\ \tau(\boldsymbol{\ell}) \end{pmatrix}. \quad (30)$$

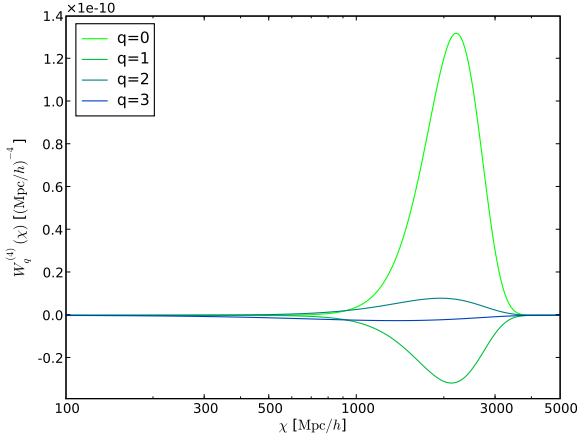


Figure 2. Line-of-sight weighting functions $W_q^{(4)}(\chi)$ for mixed iSW-galaxy trispectra as a function of comoving distance.

Mixed spectra can now be defined in a compact way

$$\begin{aligned} \langle \varphi_{i_1}(\ell_1) \varphi_{i_2}(\ell_2) \varphi_{i_3}(\ell_3) \rangle &= (2\pi)^3 \delta_D(\ell_{1\dots 3}) B_{i_1 i_2 i_3}^{\ell_1, \ell_2, \ell_3} \\ \langle \varphi_{i_1}(\ell_1) \varphi_{i_2}(\ell_2) \varphi_{i_3}(\ell_3) \varphi_{i_4}(\ell_4) \rangle &= (2\pi)^3 \delta_D(\ell_{1\dots 4}) T_{i_1 i_2 i_3 i_4}^{\ell_1, \ell_2, \ell_3, \ell_4}. \end{aligned} \quad (31)$$

3.4 Weighting functions

For a mixed n -point function, the product of the n different weighting functions, is uniquely given by the sum of the field indices q . In case of the bispectrum we would define $q = i_1 + i_2 + i_3$, whereas in case of the trispectrum $q = i_1 + i_2 + i_3 + i_4$. We can therefore define a q -dependent combined weighting function $W_q^{(n)}(\chi)$

$$W_q^{(n)}(\chi) = W_q^q(\chi) W_{\gamma}^{n-q}(\chi) \quad (32)$$

where $n = 3$ and $n = 4$ correspond to the bispectra and trispectra, respectively. The different weightings in case of the trispectra are depicted in Fig. 2 for different field mixtures q . Despite the weightings show strong differences in amplitude and sign, common to all weightings is a broad peak between 1 and 4 Gpc h^{-1} due to the maximum in the galaxy redshift distribution $p(z)$.

3.5 Time evolution

The time evolution of each linear galaxy field $\gamma(a, \mathbf{k})$ is given by the growth function $D_+(a)$. The n -th non-linear perturbative contributions evolve simply with the n -th order of the growth function D_+^n . This is not the case for the iSW field contributions $\tau(a, \mathbf{k})$. While the linear term evolves proportional to $d(D_+/a)/da$ the higher orders can not just be written as the n -th power of the linear growth but are proportional to $d(D_+^n/a)/da$.

Due to this fact, different perturbative contributions to mixed bispectra and trispectra will in general not have the same time evolution. In order to obtain a compact notation we introduce the time evolution doublet to n -th order $\mathbf{Q}^{(n)}(a)$

$$\mathbf{Q}^{(n)}(a) = \begin{pmatrix} Q_0^{(n)}(a) \\ Q_1^{(n)}(a) \end{pmatrix} = \begin{pmatrix} D_+^n \\ \frac{d}{da} \left(\frac{D_+^n}{a} \right) \end{pmatrix}. \quad (33)$$

With these time evolution functions $\mathbf{Q}^{(n)}(a)$ we are now able to write down the general mixed time evolving source fields. For the

tree-level bispectra we define

$$\begin{aligned} B_{i_1 i_2 i_3}^{\mathbf{k}_1, \mathbf{k}_2, \mathbf{k}_3} &= (\chi_H k_1)^{-2i_1} (\chi_H k_2)^{-2i_2} (\chi_H k_3)^{-2i_3} \\ &\left(Q_{i_1}^{(2)}(a) Q_{i_2}^{(1)}(a) Q_{i_3}^{(1)}(a) b_{\delta}^{\mathbf{k}_2, \mathbf{k}_3} \right. \\ &+ Q_{i_2}^{(2)}(a) Q_{i_3}^{(1)}(a) Q_{i_1}^{(1)}(a) b_{\delta}^{\mathbf{k}_3, \mathbf{k}_1} \\ &\left. + Q_{i_3}^{(2)}(a) Q_{i_1}^{(1)}(a) Q_{i_2}^{(1)}(a) b_{\delta}^{\mathbf{k}_1, \mathbf{k}_2} \right). \end{aligned} \quad (34)$$

The terms $(\chi_H k_i)^{-2i}$ are the Poisson factors from the iSW effect. In case of the tree-level trispectrum the source will consist of two contributions - one originating from second order and third order perturbation theory respectively. The time dependent source for the trispectra then reads

$$\begin{aligned} T_{i_1 i_2 i_3 i_4}^{\mathbf{k}_1, \mathbf{k}_2, \mathbf{k}_3, \mathbf{k}_4} &= (\chi_H k_1)^{-2i_1} (\chi_H k_2)^{-2i_2} (\chi_H k_3)^{-2i_3} (\chi_H k_4)^{-2i_4} \\ &\left(Q_{i_1}^{(2)}(a) Q_{i_2}^{(2)}(a) Q_{i_3}^{(1)}(a) Q_{i_4}^{(1)}(a) t_{\delta}^{(2)}(\mathbf{k}_1, \mathbf{k}_2, \mathbf{k}_3, \mathbf{k}_4) \right. \\ &+ \text{all pairs } \in \{1, 2, 3, 4\} \\ &+ Q_{i_1}^{(3)}(a) Q_{i_2}^{(1)}(a) Q_{i_3}^{(1)}(a) Q_{i_4}^{(1)}(a) t_{\delta}^{(3)}(\mathbf{k}_1, \mathbf{k}_2, \mathbf{k}_3, \mathbf{k}_4) \\ &\left. + \text{cyclic } \{1, 2, 3, 4\} \right). \end{aligned} \quad (35)$$

Now, the flat sky Limber equations for the mixed angular bispectra and trispectra read (Hu 2001)

$$\begin{aligned} B_{i_1 i_2 i_3}^{\ell_1, \ell_2, \ell_3} &= \int_0^{\chi_H} d\chi \frac{1}{\chi^4} W_q^{(3)}(\chi) B_{i_1 i_2 i_3}^{\mathbf{k}_1, \mathbf{k}_2, \mathbf{k}_3} \\ T_{i_1 i_2 i_3 i_4}^{\ell_1, \ell_2, \ell_3, \ell_4} &= \int_0^{\chi_H} d\chi \frac{1}{\chi^6} W_q^{(4)}(\chi) T_{i_1 i_2 i_3 i_4}^{\mathbf{k}_1, \mathbf{k}_2, \mathbf{k}_3, \mathbf{k}_4}, \end{aligned} \quad (36)$$

where the source field spectra are evaluated at the 3-dimensional wave vectors $\mathbf{k}_i = (l_{i,1}, l_{i,2}, 0)$. Since the weighting functions are slowly varying in comparison to the source field, fluctuations in the line-of-sight direction are smeared out by the integrations. Therefore, the fields can be assumed as non-fluctuating in this direction in the first place.

While pure spectra are invariant under exchange of wave vectors ℓ_i ,

$$\begin{aligned} B_{aaa}^{\ell_1, \ell_2, \ell_3} &= B_{aaa}^{\ell_2, \ell_3, \ell_1} = B_{aaa}^{\ell_3, \ell_1, \ell_2} \\ T_{aaaa}^{\ell_1, \ell_2, \ell_3, \ell_4} &= T_{aaaa}^{\ell_2, \ell_3, \ell_4, \ell_1} = T_{aaaa}^{\ell_3, \ell_4, \ell_1, \ell_2} = T_{aaaa}^{\ell_4, \ell_1, \ell_2, \ell_3}, \end{aligned} \quad (37)$$

this does not generally hold true for mixed spectra $B_{abc}^{\ell_a, \ell_b, \ell_c}$. However, in general, all spectra are invariant under a simultaneous exchange of wave numbers and field indices

$$\begin{aligned} B_{i_1 i_2 i_3}^{\ell_1, \ell_2, \ell_3} &= B_{i_2 i_3 i_1}^{\ell_2, \ell_3, \ell_1} = B_{i_3 i_1 i_2}^{\ell_3, \ell_1, \ell_2} \\ T_{i_1 i_2 i_3 i_4}^{\ell_1, \ell_2, \ell_3, \ell_4} &= T_{i_2 i_3 i_4 i_1}^{\ell_2, \ell_3, \ell_4, \ell_1} = T_{i_3 i_4 i_1 i_2}^{\ell_3, \ell_4, \ell_1, \ell_2} = T_{i_4 i_1 i_2 i_3}^{\ell_4, \ell_1, \ell_2, \ell_3}. \end{aligned} \quad (38)$$

These symmetries are simply caused by the commutation invariance in the products of source fields in eqn. (26).

3.6 Equilateral bispectra and square trispectra

To require homogeneity the wave vector arguments have to form a triangle, $\ell_1 + \ell_2 + \ell_3 = 0$, for the bispectrum and a quadrangle, $\ell_1 + \ell_2 + \ell_3 + \ell_4 = 0$, in case of the trispectrum. Thus, due to isotropy the scale dependence of the bispectrum is uniquely defined by the absolute values of the angular wave vectors ℓ_i

$$B_{abc}^{\ell_a, \ell_b, \ell_c} = B_{abc}^{\ell_a, \ell_b, \ell_c}. \quad (39)$$

The scale dependence of the trispectra, however, can be described by the four absolute values of the angular wave vectors ℓ_i and one diagonal L

$$T_{abc}^{\ell_a, \ell_b, \ell_c, \ell_d} = T_{abc}^{\ell_a, \ell_b, \ell_c, \ell_d, L}. \quad (40)$$

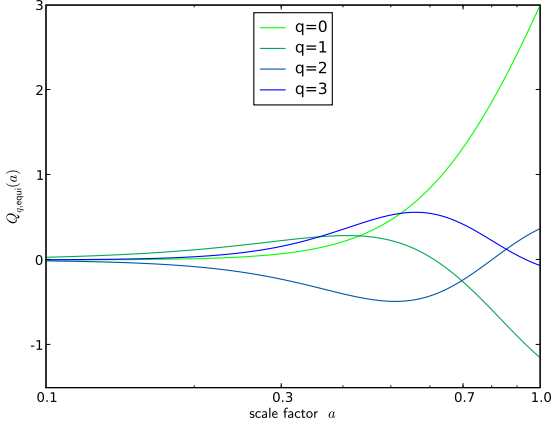


Figure 3. Time evolution functions for equilateral mixed iSW-galaxy bispectra $B_{i_1 i_2 i_3}^{\ell, \ell, \ell}$ as a function of angular scale ℓ . The value $q = i_1 + i_2 + i_3$ defines the mixture of the source fields. While the growth functions of the galaxy distribution stay positive to all perturbative orders, the derivatives in the iSW evolution functions also introduce negative terms into the evolution.

This leads to the fact that the source fields of equilateral bispectra are symmetric with respect to their field indices and have a uniform time evolution $Q_{q, \text{equi}}(a)$

$$Q_{q, \text{equi}} = \begin{cases} D_+^3 & (q=0) \\ \frac{1}{3} D_+^2 \left(\frac{d}{da} \frac{D_+^2}{a} \right) + \frac{2}{3} D_+^3 \left(\frac{d}{da} \frac{D_+}{a} \right) & (q=1) \\ \frac{2}{3} D_+ \left(\frac{d}{da} \frac{D_+^2}{a} \right) \left(\frac{d}{da} \frac{D_+}{a} \right) + \frac{1}{3} D_+^3 \left(\frac{d}{da} \frac{D_+}{a} \right)^2 & (q=2) \\ \left(\frac{d}{da} \frac{D_+^2}{a} \right) \left(\frac{d}{da} \frac{D_+}{a} \right)^2 & (q=3) \end{cases} \quad (41)$$

These time evolutions are depicted in Fig. 3. While the growth functions of the galaxy distribution stay positive to all perturbative orders, the derivatives in the iSW evolution functions also introduce negative terms into the evolution. This will later lead to a change from correlation to anti-correlation along the line-of-sight.

Slightly more complex is the time evolution for source fields of the square trispectra. Here, the contributions from second order perturbation theory evolve still differently compared to the third order terms. The second order terms $Q_{q, \text{square}}^{(2)}(a)$ read

$$Q_{q, \text{square}}^{(2)} = \begin{cases} D_+^6 & (q=0) \\ \frac{1}{2} D_+^4 \left(\frac{d}{da} \frac{D_+^2}{a} \right) + \frac{1}{2} D_+^5 \left(\frac{d}{da} \frac{D_+}{a} \right) & (q=1) \\ \frac{1}{6} D_+^4 \left(\frac{d}{da} \frac{D_+}{a} \right)^2 + \frac{2}{3} D_+^3 \left(\frac{d}{da} \frac{D_+^2}{a} \right) \left(\frac{d}{da} \frac{D_+}{a} \right) \\ + \frac{1}{6} D_+^2 \left(\frac{d}{da} \frac{D_+^2}{a} \right)^2 & (q=2) \\ \frac{1}{2} D_+ \left(\frac{d}{da} \frac{D_+^2}{a} \right)^2 \left(\frac{d}{da} \frac{D_+}{a} \right) + \frac{1}{2} D_+^2 \left(\frac{d}{da} \frac{D_+^2}{a} \right) \left(\frac{d}{da} \frac{D_+}{a} \right)^2 & (q=3) \\ \left(\frac{d}{da} \frac{D_+^2}{a} \right)^2 \left(\frac{d}{da} \frac{D_+}{a} \right)^2 & (q=4) \end{cases}$$

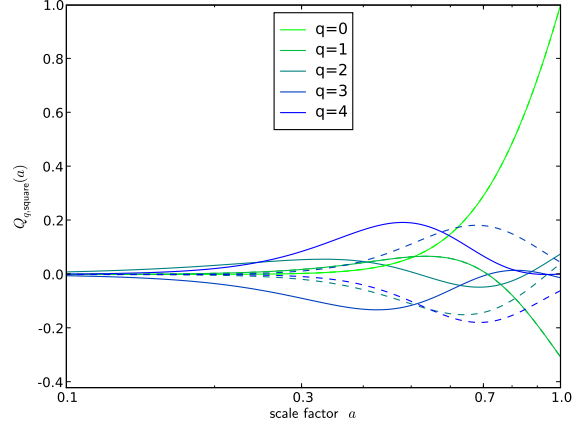


Figure 4. Time evolution functions for square mixed iSW-galaxy trispectra $T_{(i_1 i_2 i_3 i_4)}^{\ell, \ell, \ell, \ell, \sqrt{2}\ell}$ as a function of angular scale ℓ . The value $q = i_1 + i_2 + i_3 + i_4$ defines the mixture of the source fields. The solid lines depict the second order perturbative time evolutions $Q_{q, \text{square}}^{(2)}$, the third order terms $Q_{q, \text{square}}^{(3)}$ are shown as dashed lines. While the growth functions of the galaxy distribution stay positive to all perturbative orders, the derivatives in the iSW evolution functions also introduce negative terms into the evolution.

and for the third order we obtain the following time evolution:

$$Q_{q, \text{square}}^{(3)} = \begin{cases} D_+^6 & (q=0) \\ \frac{1}{4} D_+^5 \left(\frac{d}{da} \frac{D_+}{a} \right) + \frac{3}{4} D_+^3 \left(\frac{d}{da} \frac{D_+^3}{a} \right) & (q=1) \\ \frac{1}{2} D_+^4 \left(\frac{d}{da} \frac{D_+}{a} \right)^2 + \frac{1}{2} D_+^2 \left(\frac{d}{da} \frac{D_+^3}{a} \right) \left(\frac{d}{da} \frac{D_+}{a} \right) & (q=2) \\ \frac{1}{4} D_+^3 \left(\frac{d}{da} \frac{D_+^2}{a} \right)^3 + \frac{3}{4} D_+ \left(\frac{d}{da} \frac{D_+^3}{a} \right) \left(\frac{d}{da} \frac{D_+}{a} \right)^2 & (q=3) \\ \left(\frac{d}{da} \frac{D_+^3}{a} \right) \left(\frac{d}{da} \frac{D_+}{a} \right)^3 & (q=4) \end{cases}$$

In time evolutions for the different perturbative orders of the mixed trispectra are depicted in Fig. 4. One can see that for $q = 1, 2$ they evolve identically but differ stronger with increasing number q of included iSW fields.

The equilateral bispectra and square trispectra are depicted in Fig. 5 and Fig. 6. As in the power spectra one can observe also here the weakness of the iSW signal in comparison to the projected galaxy distribution field. This is clearly shown in the decrease of the polyspectra with increasing number q of included iSW source fields. Once more, the iSW effect shows its nature of being a large scale effect. With higher q the slope of the spectra increases in the large ℓ region. The physical reason for this is the coupling of the iSW effect to the gravitational potential in contrast to the galaxy distribution, which couples directly to the density contrast. Mathematically, this fact manifests itself in the appearance of the $1/k^2$ factors for the iSW contributions, originating from the inversion of the Poisson equation.

While the linear iSW effect is strictly anti-correlated with respect to the galaxy density, cross-spectra with this linear signal would never show a change in sign in dependence on ℓ . This does not hold true any longer for the non-linear iSW effect. The higher order contributions now have the opposite sign in their time evolution. It is therefore possible that for large ℓ the linear effect dominates while for small ℓ the non-linear effect determines the sign of the correlation. These changes in sign in dependence of ℓ can now be observed in Fig. 5 and Fig. 6, for instance at $\ell \approx 80$ in the bis-

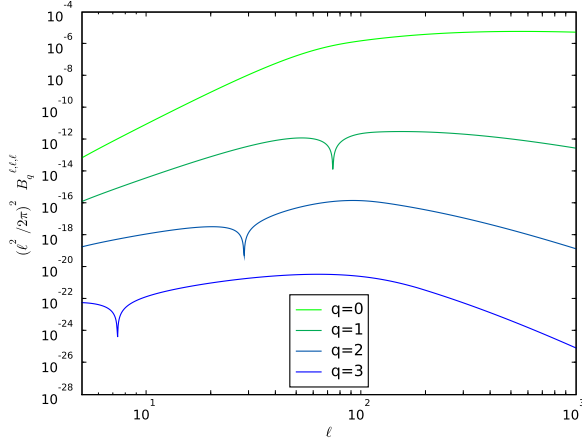


Figure 5. The absolute values of the mixed equilateral iSW-galaxy bispectra $B_{i_1 i_2 i_3}^{\ell, \ell, \ell}$ as a function of angular scale ℓ are depicted in this figure. The value $q = i_1 + i_2 + i_3$ defines the mixture of the source fields.

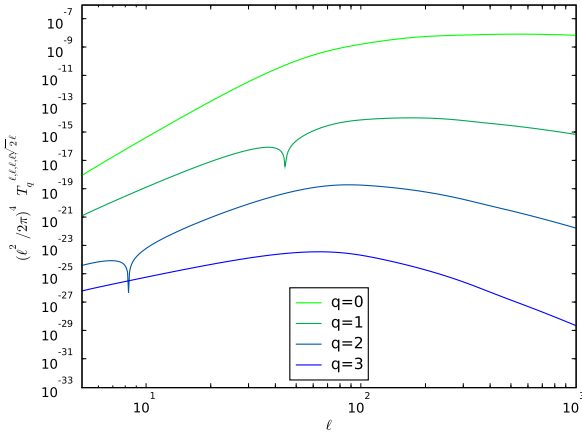


Figure 6. The absolute values of the mixed square iSW-galaxy trispectra $T_{i_1 i_2 i_3 i_4}^{\ell, \ell, \ell, \ell, \sqrt{2}\ell}$ as a function of angular scale ℓ are shown in this plot. The value $q = i_1 + i_2 + i_3 + i_4$ defines the mixture of the source fields.

spectrum $\langle \tau \gamma^2 \rangle$. This behavior has also been observed and studied in the CMB-weak-lensing cross spectrum (Nishizawa et al. 2008).

4 DETECTABILITY

4.1 Sources of noise

The step from a good theoretical framework to an analysis of real data or to an estimation of the realistically accessible information content encompasses the description of all relevant effects influencing the measured data. Only then, one will be able to make statements about a physical process and the likelihood of its actual measurement. For the evaluation of the covariances of the bispectra and trispectra, the two-point function will be needed. In the same notation as the higher order spectra their are defined as

$$\langle \varphi_{i_1}(\ell_1) \varphi_{i_2}(\ell_2) \rangle = (2\pi)^2 \delta_{\mathbb{D}}(\ell_1 + \ell_2) C_{i_1 i_2}^{\ell_1} \quad (42)$$

In the case at hand the actual theoretically expected iSW signal in our fiducial cosmological model is superposed to the primary CMB

N	$\Delta\Omega$	f_{sky}	z_0	b	n
3.0×10^9	2π	0.5	0.64	1.0	4.7×10^8

Table 1. The Properties of the *Euclid* galaxy survey are listed in this table: total number N of objects, solid angle $\Delta\Omega$ covered (in radians), sky fraction f_{sky} , redshift parameter z_0 , galaxy bias b and density per unit steradian n .

fluctuations. Its relative amplitude reaches from 10% on very large scales to an negligible fraction of the signal for scales smaller than $\ell \approx 200$. Furthermore, the detected CMB signal is subjected to instrumental noise σ_τ and a Gaussian beam $\beta(\ell)$.

Assuming that the noise sources of the galaxy counts are mutually uncorrelated, the pure galaxy-galaxy spectra are solely subjected to a Poissonian noise term n^{-1} .

The cross-spectra between the two fields will be free of noise, since the noise sources of the single fields are uncorrelated.

Now we can relate the measured spectra $\tilde{C}_{i_1 i_2}^\ell$ to the theoretical spectra $\tilde{C}_{i_1 i_2}^\ell$:

$$\begin{aligned} \tilde{C}_{00}^\ell &= C_{00}^\ell + n^{-1} \\ \tilde{C}_{01}^\ell &= C_{01}^\ell \\ \tilde{C}_{11}^\ell &= C_{11}^\ell + C_{\text{CMB}}^\ell + \sigma_\tau^2 \beta^{-2}(\ell). \end{aligned} \quad (43)$$

The contributions in detail are:

(i) As the Fourier transform of the Gaussian beam one obtains $\beta^{-2}(\ell) = \exp(\Delta\theta^2 \ell(\ell + 1))$. We use $\Delta\theta = 7.1$ arcmin, which corresponds to the $\nu = 143$ GHz channels closest to the CMB emission maximum. For the conversion of $w_T^{-1} = T_{\text{CMB}}^2 \sigma_\tau^2$ to the noise amplitude in the dimensionless temperature perturbation τ with $w_T = (0.01 \mu\text{K})^2$ (Zaldarriaga et al. 1997) we use the value $T_{\text{CMB}} = 2.725$ K for the CMB temperature.

(ii) Furthermore, a CMB temperature power spectrum $C_{\text{CMB}}(\ell)$ was generated, which was equally scaled with the CMB temperature $T_{\text{CMB}} = 2.725$ K, with the Code for Anisotropies in the Microwave Background (CAMB, Lewis et al. 2000) for the fiducial ΛCDM cosmology. The noise contribution from the CMB-spectrum C_{CMB}^ℓ represents the main challenge in the observation of the iSW bispectra and trispectra. It provides high values for the covariance at low multipoles ℓ , and it by far dominates $\tilde{C}_{00}(\ell)$, $C_{\text{CMB}} \gg C_{00}(\ell)$ on the angular scales considered. The orders of magnitude for the different contributions of the linear estimator \tilde{C}_{11}^ℓ are depicted in Fig 7. One can see, that even at large angular scales ℓ the pure iSW signal C_{11}^ℓ is still more than one order of magnitude weaker than the signal from primordial fluctuations C_{CMB}^ℓ .

(iii) The inverse number density n of objects per unit steradian determines the Poissonian noise term in the galaxy count. In Table 4.1 the properties of the main galaxy sample as it would be expected from *Euclid* are summarized. Major advantages lie in the large sky coverage and the high number of observed objects. Here, we assumed a non-evolving galaxy bias for simplicity.

4.2 Covariances

In the case of Gaussian noise the observed and estimated bispectra $\tilde{B}_{i_1 i_2 i_3}^{\ell_1, \ell_2, \ell_3}$ and the trispectra $\tilde{T}_{i_1 i_2 i_3 i_4}^{\ell_1, \ell_2, \ell_3, \ell_4}$ are unbiased estimates of the true bispectra $B_{i_1 i_2 i_3}^{\ell_1, \ell_2, \ell_3}$ and trispectra $T_{i_1 i_2 i_3 i_4}^{\ell_1, \ell_2, \ell_3, \ell_4}$ (Hu 2001),

$$\begin{aligned} \tilde{B}_{i_1 i_2 i_3}^{\ell_1, \ell_2, \ell_3} &\simeq B_{i_1 i_2 i_3}^{\ell_1, \ell_2, \ell_3} \\ \tilde{T}_{i_1 i_2 i_3 i_4}^{\ell_1, \ell_2, \ell_3, \ell_4} &\simeq T_{i_1 i_2 i_3 i_4}^{\ell_1, \ell_2, \ell_3, \ell_4}. \end{aligned} \quad (44)$$

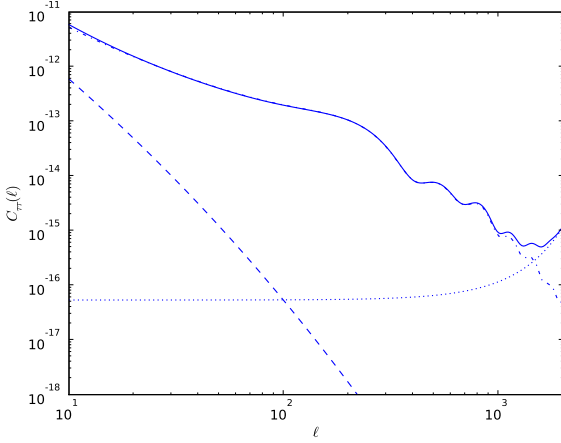


Figure 7. Constituents of the measured angular CMB spectrum \tilde{C}_{11}^{ℓ} . Depicted are the total signal \tilde{C}_{11}^{ℓ} (solid line), the contribution from primordial fluctuations C_{CMB}^{ℓ} , the iSW-effect C_{11}^{ℓ} and the instrumental noise $\sigma_7^2 \beta^{-2}(\ell)$, which is fortunately sub-dominant at the large scales of interest.

This is in contrast to the spectra $C_{i_1 i_2}^{\ell}$, which were discussed in the previous subsection. The covariances of the estimators of the bispectra and trispectra are defined as

$$\begin{aligned} & \text{Cov} \left[\tilde{B}_{i_1 i_2 i_3}^{\ell_1, \ell_2, \ell_3}, \tilde{B}_{i_1 i_2 i_3}^{\ell'_1, \ell'_2, \ell'_3} \right] \\ &= \left\langle \left(\tilde{B}_{i_1 i_2 i_3}^{\ell_1, \ell_2, \ell_3} - B_{i_1 i_2 i_3}^{\ell_1, \ell_2, \ell_3} \right) \left(\tilde{B}_{i_1 i_2 i_3}^{\ell'_1, \ell'_2, \ell'_3} - B_{i_1 i_2 i_3}^{\ell'_1, \ell'_2, \ell'_3} \right) \right\rangle, \\ & \text{Cov} \left[\tilde{T}_{i_1 i_2 i_3 i_4}^{\ell_1, \ell_2, \ell_3, \ell_4}, \tilde{T}_{i_1 i_2 i_3 i_4}^{\ell'_1, \ell'_2, \ell'_3, \ell'_4} \right] \\ &= \left\langle \left(\tilde{T}_{i_1 i_2 i_3 i_4}^{\ell_1, \ell_2, \ell_3, \ell_4} - T_{i_1 i_2 i_3 i_4}^{\ell_1, \ell_2, \ell_3, \ell_4} \right) \left(\tilde{T}_{i_1 i_2 i_3 i_4}^{\ell'_1, \ell'_2, \ell'_3, \ell'_4} - T_{i_1 i_2 i_3 i_4}^{\ell'_1, \ell'_2, \ell'_3, \ell'_4} \right) \right\rangle. \quad (45) \end{aligned}$$

In a Gaussian approximation, which we are using here, any covariances can be expressed as a sum of products of two-point functions using Wick's theorem. While for pure covariances only the respective power spectra appear in this expansion, in our case of mixed covariances the products are formed from the estimators of the cross-correlation \tilde{C}_{01}^{ℓ} and the two auto-correlations \tilde{C}_{00}^{ℓ} and \tilde{C}_{11}^{ℓ} .

In case of the bispectra with mutually unequal angular wave numbers $\ell_j \neq \ell_k$ for $j \neq k$ the covariance can be written as a sum over terms which are cubic in the spectra $C_{i_1 i_2}^{\ell}$

$$\begin{aligned} & \text{Cov} \left[\tilde{B}_{abc}^{\ell_1, \ell_2, \ell_3}, \tilde{B}_{a'b'c'}^{\ell'_1, \ell'_2, \ell'_3} \right] \\ &= \tilde{C}_{aa'}^{\ell_1} \tilde{C}_{bb'}^{\ell_2} \tilde{C}_{cc'}^{\ell_3} \delta_{\text{D}}(\ell_1 - \ell'_1) \delta_{\text{D}}(\ell_2 - \ell'_2) \delta_{\text{D}}(\ell_3 - \ell'_3) \\ & \quad + \text{perm}(\ell'_1, \ell'_2, \ell'_3). \quad (46) \end{aligned}$$

On the subspace $\ell_1, \ell'_1 < \ell_2, \ell'_2 < \ell_3, \ell'_3$ only the first term is non-vanishing. This block-diagonal matrix can now be inverted to

$$\begin{aligned} & \text{Cov}^{-1} \left[\tilde{B}_{abc}^{\ell_1, \ell_2, \ell_3}, \tilde{B}_{a'b'c'}^{\ell'_1, \ell'_2, \ell'_3} \right] = \frac{\tilde{C}_{aa'}^{\ell_1} \tilde{C}_{bb'}^{\ell_2} \tilde{C}_{cc'}^{\ell_3}}{\det C^{\ell_1} \det C^{\ell_2} \det C^{\ell_3}} \\ & \quad \times \delta_{\text{D}}(\ell_1 - \ell'_1) \delta_{\text{D}}(\ell_2 - \ell'_2) \delta_{\text{D}}(\ell_3 - \ell'_3), \quad (47) \end{aligned}$$

with the adjoint matrix $\tilde{C}_{aa'}^{\ell}$,

$$\tilde{C}_{aa'}^{\ell} = \begin{pmatrix} C_{11}^{\ell} & -C_{01}^{\ell} \\ -C_{01}^{\ell} & C_{00}^{\ell} \end{pmatrix}. \quad (48)$$

In analogy to the bispectrum case, the inverse covariance of the

q	0	1	2
$\Sigma_q^{(3)}$	87.8	0.828	$4.43 \cdot 10^{-3}$
$\Sigma_q^{(4)}$	21.7	0.19	$1.42 \cdot 10^{-3}$

Table 2. Cumulative signal-to-noise ratios $\Sigma_q^{(n)}$ for measurements of the bispectra $\langle \tau^q \gamma^{3-q} \rangle$ and the trispectra $\langle \tau^q \gamma^{4-q} \rangle$, $q = 0, 1, 2$, for *Planck* CMB data in cross-correlation with *Euclid*-like survey, up to a resolution limit $\ell_{\text{max}} = 10^3$ starting from a minimum angular wave number of $\ell_{\text{min}} = 10$.

trispectra in the subspace $\ell_1, \ell'_1 < \ell_2, \ell'_2 < \ell_3, \ell'_3 < \ell_4, \ell'_4$ amounts to

$$\begin{aligned} & \text{Cov}^{-1} \left[\tilde{T}_{abcd}^{\ell_1, \ell_2, \ell_3, \ell_4}, \tilde{T}_{a'b'c'd'}^{\ell'_1, \ell'_2, \ell'_3, \ell'_4} \right] = \frac{\tilde{C}_{aa'}^{\ell_1} \tilde{C}_{bb'}^{\ell_2} \tilde{C}_{cc'}^{\ell_3} \tilde{C}_{dd'}^{\ell_4}}{\det C^{\ell_1} \det C^{\ell_2} \det C^{\ell_3} \det C^{\ell_4}} \\ & \quad \times \delta_{\text{D}}(\ell_1 - \ell'_1) \delta_{\text{D}}(\ell_2 - \ell'_2) \delta_{\text{D}}(\ell_3 - \ell'_3) \delta_{\text{D}}(\ell_4 - \ell'_4). \quad (49) \end{aligned}$$

For an observation covering the sky with a fraction of f_{sky} the covariances scale like f_{sky}^{-1} . The anti-correlation in the cross-spectra C_{01}^{ℓ} will not change the sign of the covariances, since in each of the products an even number of these mixed spectra appears.

4.3 Signal-to-noise ratios

The signal-to-noise ratio $\Sigma^{(3)}$ for the simultaneous measurements of the all pure and mixed bispectra $\langle \tau^q \gamma^{3-q} \rangle$ and $\Sigma_q^{(4)}$ for the all mixed and pure trispectra $\langle \tau^q \gamma^{4-q} \rangle$, where all field indices are summed over, would imply a thorough derivation of all cross-correlations between different field mixtures. Here, we are rather interested in the individual signal-to-noise ratios of certain field configurations. If one reduces the data to a mixed configuration q , only the cases $q = 0$ and $q = 1$ provide measurement in and above the detection limit. For $q = 0$ we obtain

$$\begin{aligned} (\Sigma_0^{(3)})^2 &= \frac{f_{\text{sky}}}{4\pi^3} \int d^2 \ell_1 d^2 \ell_2 \frac{(B_{000}^{\ell_1, \ell_2, \ell_3})^2}{6 \tilde{C}_{00}^{\ell_1} \tilde{C}_{00}^{\ell_2} \tilde{C}_{00}^{\ell_3}} \\ (\Sigma_0^{(4)})^2 &= \frac{f_{\text{sky}}}{8\pi^4} \int d^2 \ell_1 d^2 \ell_2 d^2 \ell_3 \frac{(T_{0000}^{\ell_1, \ell_2, \ell_3, \ell_4})^2}{24 \tilde{C}_{00}^{\ell_1} \tilde{C}_{00}^{\ell_2} \tilde{C}_{00}^{\ell_3} \tilde{C}_{00}^{\ell_4}} \quad (50) \end{aligned}$$

However, since we are aiming for iSW detections, the more interesting case is $q = 1$. The signal-to-noise ratio then splits up into two contributions,

$$\begin{aligned} (\Sigma_1^{(3)})^2 &= \frac{f_{\text{sky}}}{4\pi^3} \int d^2 \ell_1 d^2 \ell_2 \left(2 \det C^{\ell_1} \det C^{\ell_2} \det C^{\ell_3} \right)^{-1} \\ & \quad \left[(B_{001}^{\ell_1, \ell_2, \ell_3})^2 \tilde{C}_{11}^{\ell_1} \tilde{C}_{11}^{\ell_2} \tilde{C}_{00}^{\ell_3} + B_{001}^{\ell_1, \ell_2, \ell_3} \tilde{C}_{11}^{\ell_1} \tilde{C}_{01}^{\ell_2} \tilde{C}_{01}^{\ell_3} B_{010}^{\ell_1, \ell_2, \ell_3} \right] \\ (\Sigma_1^{(4)})^2 &= \frac{f_{\text{sky}}}{8\pi^4} \int d^2 \ell_1 d^2 \ell_2 d^2 \ell_3 \left(\det C^{\ell_1} \dots \det C^{\ell_4} \right)^{-1} \\ & \quad \left[\frac{1}{6} (T_{0001}^{\ell_1, \ell_2, \ell_3, \ell_4})^2 \tilde{C}_{11}^{\ell_1} \tilde{C}_{11}^{\ell_2} \tilde{C}_{11}^{\ell_3} \tilde{C}_{00}^{\ell_4} \right. \\ & \quad \left. + \frac{1}{4} T_{0001}^{\ell_1, \ell_2, \ell_3, \ell_4} \tilde{C}_{11}^{\ell_1} \tilde{C}_{11}^{\ell_2} \tilde{C}_{01}^{\ell_3} \tilde{C}_{01}^{\ell_4} T_{0010}^{\ell_1, \ell_2, \ell_3, \ell_4} \right]. \quad (51) \end{aligned}$$

A detailed calculation of the signal-to noise expressions can be found in Section A. The inverse covariances of the polyspectra will always remain positive, since always an even number of anti-correlating cross-spectra will appear in its expression. However, the mixed field contributions can in general become negative.

The cumulative signal-to-noise ratios $\Sigma_q^{(n)}$ for the mixed bispectra B_q and the mixed trispectra T_q are depicted in Fig. 8 for the pure galaxy spectra and spectra with up to two iSW source fields included, $q = 0, 1, 2$.

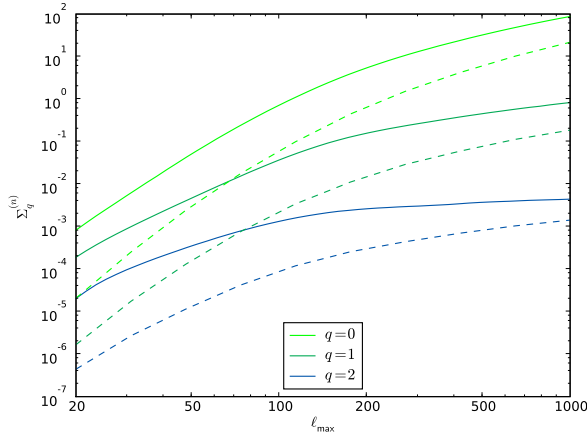


Figure 8. Cumulative signal-to-noise ratios $\Sigma_q^{(n)}$ for measurements of the bispectra $\langle \tau^q \gamma^{3-q} \rangle$ (solid lines) and the trispectra $\langle \tau^q \gamma^{4-q} \rangle$ (dashed lines), $q = 0, 1$, for *Planck* CMB data in cross-correlation with *Euclid*-like survey, up to a resolution limit $\ell_{\max} = 10^3$ starting from a minimum angular wave number of $\ell_{\min} = 10$.

The qualitative behavior of the cumulative signal-to-noise curves are again determined by the individual signal strengths of the two source fields γ and τ . The strong fluctuation of the galaxy distribution γ even on small scales leads to a considerable increase of Σ for large ℓ and small q . In contrast to this the iSW-effect is a large scale effect and therefore increases the slope in the small ℓ limit of the spectrum. It does not contribute significant signal strength above values of $\ell_{\max} > 300$, for this reason the signal-to-noise curves flatten off in this region of the spectrum for $q = 1, 2$. The wider spread between different values of q for the trispectrum in contrast to the bispectrum is due to the higher power of source fields.

Quantitatively, higher values of q lead to smaller significance in the signal. Included were contributions starting from large angular scales $\ell_{\min} = 10$ up to smallest scales measurable in the *Planck* survey $\ell_{\max} = 10^3$. The pure galaxy polyspectra $\langle \gamma^3 \rangle$ and $\langle \gamma^4 \rangle$ can both be measured with a detection significance of $\gg 3\sigma$, $\Sigma_0^{(3)} = 87.8$ and $\Sigma_0^{(4)} = 21.7$. Including only one iSW source field reduces the signal down to the noise level. While the bispectrum $\langle \tau \gamma^2 \rangle$ reaches a signal-to-noise ratio of 0.82, the value for the trispectrum $\langle \tau \gamma^3 \rangle$ reaches a maximum of 0.19. Combining measurements of the $q = 1$ bi- and trispectra would therefore be able to contribute a maximum signal-to-noise contribution of $\Sigma \approx 0.84$. Unfortunately, this is - taken on its own - still a very poor measurement significance. However, it could be used as an additional signal source to the strongest iSW signal from the cross spectrum $\langle \tau \gamma \rangle$.

For the higher values of q only the case of two iSW source fields $q = 2$ is plotted in Fig. 8. Both for the bispectrum as well as for the trispectra the signal-to-noise ratios are negligible with maximum values of $4.43 \cdot 10^{-3}$ and $1.42 \cdot 10^{-3}$ respectively.

One can obtain a grasp of the differential contributions of the signal-to-noise ratios with respect to angular scale ℓ , if one studies the quantity

$$\begin{aligned} \left(\frac{d}{d\ell} \Sigma_{q,\text{equi}}^{(3)} \right)^{\frac{1}{2}} &\propto B_q^{\ell,\ell,\ell} \sqrt{\text{Cov}^{-1} \left(B_q^{\ell,\ell,\ell} \right)} \\ \left(\frac{d}{d\ell} \Sigma_{q,\text{square}}^{(4)} \right)^{\frac{1}{2}} &\propto T_q^{\ell,\ell,\ell,\ell, \sqrt{2}\ell} \sqrt{\text{Cov}^{-1} \left(T_q^{\ell,\ell,\ell,\ell, \sqrt{2}\ell} \right)}. \end{aligned} \quad (52)$$

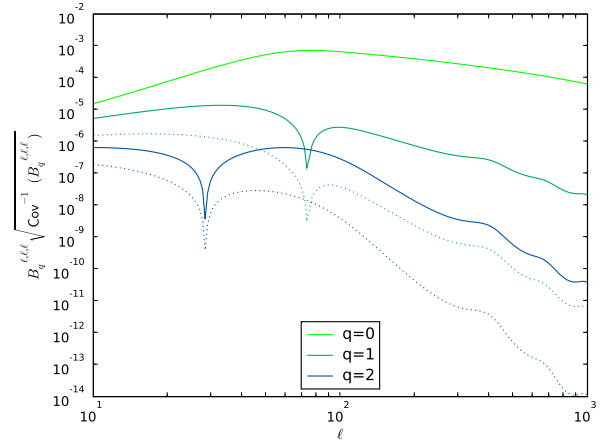


Figure 9. The differential contributions of the equilateral bispectra to the signal-to-noise ratios in dependence on angular wave number ℓ are depicted here for different source field mixtures $q = 0, 1, 2$ (solid lines). For $q = 1, 2$ the contributions from cross-correlations are also shown (dotted lines), as they appear for $q = 1$ in the second term of the second line in eqn. (51). One can observe the increasing amplitude of the baryonic acoustic oscillations for larger q . Also the change in sign can be studied due to the transition from linear dominated to non-linear dominated scales.

In Fig. 9 this differential contribution of equilateral bispectra in dependence on ℓ are depicted for different source field mixtures q . The differential contributions of the square trispectra behave qualitatively analogous. Also the change in sign can be studied due to the transition from linear dominated to non-linear dominated scales. For $q = 1, 2$ the contributions from cross-correlations are also shown (dotted lines), as they appear for $q = 1$ in the second term of the second line in eqn. (51). As one can see, these terms are subdominant and can be neglected in our case.

One can observe the increasing amplitude of the baryonic acoustic oscillations for larger q , which originate from C_{CMB}^{ℓ} . The falling slopes of the BAO features in the covariance lead to small plateaus in the differential contributions for larger ℓ . Since in these regions the signal decreases more gently than the covariance, one obtains a local increase of signal-to-noise. However, this effect can hardly be observed in Fig. 8.

5 SUMMARY

The objective of this work is a study of the detectability of non-Gaussian signatures in non-linear iSW-effect. Besides the mixed bispectra of the form $\langle \tau^q \gamma^{3-q} \rangle$, $q = 0, 1, 2$, between the galaxy distribution γ and the iSW temperature perturbation τ we also calculate for the first time the mixed trispectra of the analogous form $\langle \tau^q \gamma^{4-q} \rangle$. Both types of spectra were consistently derived in tree-level perturbation theory in Newtonian gravity. This implies for the bispectra perturbative corrections to second order and for the mixed trispectra contributions from second and third order terms. Furthermore, we investigated the time evolution of these individual 3-dimensional source terms, which are in general very diverse. For this reason, the time evolution and the configuration dependence of a specific class of spectra, equilateral bispectra and the square trispectra, were studied. Finally, the achievable signal-to-noise ratios were derived for measurements cross-correlating *Planck* data

and a galaxy sample, as it would be expected from a wide angle survey as *Euclid*.

(i) The linear iSW-effect has the time dependence $d(D_+/a)/da$, which makes it sensitive to dark energy but vanishes in Λ CDM-models with $\Omega_m \equiv 1$ and $D_+(a) = a$. In contrast to this, the non-linear contributions to the iSW signal are sensitive to derivatives of higher powers of $D_+(a)$, namely $d(D_+^2/a)/da$ for second order perturbation theory and $d(D_+^3/a)/da$ for third order contributions. For this reason, the effect does not vanish in matter-dominated epochs.

(ii) The covariances of the measurements were derived in a Gaussian approximation. For the CMB observation the intrinsic CMB fluctuations and instrumental noise in form of the pixel noise and a Gaussian beam were considered as noise sources. A Poissonian noise term was added to the galaxy distribution signal. For simplicity the fluctuations of the dark matter density and galaxy number density were related to each other by a constant linear biasing model.

(iii) In the mixed bispectra and trispectra the configuration and scale dependence represent the different correlation lengths of the gravitational potential and the density field. Since the specific perturbative corrections dominate on different scales, the mixed spectra change their sign at certain values of ℓ . In case of the bispectra one can observe the transition from linear domination to non-linear domination move to larger and larger scales with increasing number of included iSW source fields q .

(iv) We derived the cumulative signal-to-noise ratios $\Sigma_q^{(3)}$ for the measurements of mixed bispectra $\langle \tau^q \gamma^{3-q} \rangle$, and $\Sigma_q^{(4)}$ for the mixed trispectra of the form $\langle \tau^q \gamma^{4-q} \rangle$, with a Gaussian approximation to the covariance. The integration were performed numerically using Monte Carlo integration techniques from the multidimensional numerical integration library CUBA (Hahn 2005). For both spectra the initial CMB fluctuations are the most important noise source, which makes it difficult to observe the signals. We assumed a cross-correlation of *Planck* data with a *Euclid*-like galaxy sample starting from angular scales of $\ell_{\min} = 10$ up to a resolution of $\ell_{\max} = 10^3$. The only spectra reaching the order of magnitude of the noise level are the bispectra and trispectra in the configuration $\langle \tau \gamma^{n-1} \rangle$. We found the numerical signal-to-noise ratios of $\Sigma_1^{(3)} = 0.828$ for the bispectrum and $\Sigma_1^{(4)} = 0.19$ for the trispectrum and conclude, that non-Gaussian signatures of the iSW-effect are too weak to be detected. At the same time, these small signal-to-noise ratios suggest that non-Gaussianities in the CMB generated by the iSW-effect are small enough so that they do not interfere with the estimation of the inflationary non-Gaussianity parameter f_{NL} from the bispectrum $\langle \tau^3 \rangle$ and of the two parameters g_{NL} and τ_{NL} from the trispectrum $\langle \tau^4 \rangle$.

ACKNOWLEDGEMENTS

We would like to thank Matthias Bartelmann for useful discussions and ideas. Our work was supported by the German Research Foundation (DFG) within the framework of the Priority Programme 1177 and the excellence initiative through the Heidelberg Graduate School of Fundamental Physics.

REFERENCES

Abramowitz M., Stegun I. A., 1972, Handbook of Mathematical Functions

- Aghanim N., Majumdar S., Silk J., 2008, Reports on Progress in Physics, 71, 066902
- Bardeen J. M., Bond J. R., Kaiser N., Szalay A. S., 1986, ApJ, 304, 15
- Bernardeau F., Colombi S., Gaztañaga E., Scoccimarro R., 2002, Physics Reports, 367, 1
- Boughn S., Crittenden R., 2004, Nature, 427, 45
- Boughn S. P., Crittenden R. G., Turok N. G., 1998, New Astronomy, 3, 275
- Cooray A., 2002, Phys. Rev. D, 65, 083518
- Crittenden R. G., Turok N., 1996, Physical Review Letters, 76, 575
- Fixsen D. J., 2009, ApJ, 707, 916
- Giannantonio T., Scranton R., Crittenden R. G., Nichol R. C., Boughn S. P., Myers A. D., Richards G. T., 2008, Phys. Rev. D, 77, 123520
- Goroff M. H., Grinstein B., Rey S.-J., Wise M. B., 1986, ApJ, 311, 6
- Hahn T., 2005, Computer Physics Communications, 168, 78
- Hernández-Monteagudo C., 2010, A&A, 520, A101
- Hu W., 2000, Phys. Rev. D, 62, 043007
- Hu W., 2001, Phys. Rev. D, 64, 083005
- Jain B., Bertschinger E., 1994, ApJ, 431, 495
- Lewis A., Challinor A., Lasenby A., 2000, ApJ, 538, 473
- Limber D. N., 1953, ApJ, 117, 134
- Linder E. V., Jenkins A., 2003, MNRAS, 346, 573
- López-Corredoira M., Sylos Labini F., Betancort-Rijo J., 2010, A&A, 513, A3
- Lue A., Scoccimarro R., Starkman G., 2004, Phys. Rev. D, 69, 0444005
- Martinez-Gonzalez E., Sanz J. L., Silk J., 1994, ApJ, 436, 1
- McEwen J. D., Vielva P., Hobson M. P., Martínez-González E., Lasenby A. N., 2007, MNRAS, 376, 1211
- Mo H. J., Jing Y. P., White S. D. M., 1997, MNRAS, 284, 189
- Nishizawa A. J., Komatsu E., Yoshida N., Takahashi R., Sugiyama N., 2008, ApJL, 676, L93
- Ostriker J. P., Vishniac E. T., 1986, ApJL, 306, L51
- Rees M. J., Sciama D. W., 1968, Nature, 217, 511
- Sachs R. K., Wolfe A. M., 1967, ApJ, 147, 73
- Sahni V., Coles P., 1995, Physics Reports, 262, 1
- Sanz J. L., Martínez-González E., Cayon L., Silk J., Sugiyama N., 1996, ApJ, 467, 485
- Schäfer B. M., 2008, MNRAS, 388, 1394
- Schäfer B. M., Bartelmann M., 2006, MNRAS, 369, 425
- Seljak U., 1996, ApJ, 460, 549
- Sheth R. K., Mo H. J., Tormen G., 2001, MNRAS, 323, 1
- Smail I., Hogg D. W., Blandford R., Cohen J. G., Edge A. C., Djorgovski S. G., 1995, MNRAS, 277, 1
- Spergel D. N., Verde L., Peiris H. V., Komatsu E., Nolte M. R., Bennett C. L., Halpern M., Hinshaw G., Jarosik N., Kogut A., Limon M., Meyer S. S., Page L., Tucker G. S., Weiland J. L., Wollack E., Wright E. L., 2003, ApJS, 148, 175
- Sugiyama N., 1995, ApJS, 100, 281
- Tuluie R., Laguna P., 1995, ApJL, 445, L73
- Turner M. S., White M., 1997, Phys. Rev. D, 56, 4439
- Vielva P., Martínez-González E., Tucci M., 2006, MNRAS, 365, 891
- Wang L., Steinhardt P. J., 1998, ApJ, 508, 483
- Zaldarriaga M., Spergel D. N., Seljak U., 1997, ApJ, 488, 1
- Zeldovich Y. B., Sunyaev S. R. A., 1980, Pis ma Astronomicheskii Zhurnal, 6, 737
- Zhang P., 2006, Phys. Rev. D, 73, 123504

APPENDIX A: ANALYTICAL DETAILS OF SIGNAL-TO-NOISE RATIOS

The squared signal-to-noise ratio Σ^2 is given by the χ^2 between a detection and its zero hypothesis. In the course of its calculation, one has to ensure that no redundant information is taken into account. We present the calculation for the bispectra only, since it follows the same argumentation in the case of the trispectra. Neglecting redundancy due to any symmetries all mixed and pure bispectra would account for a χ^2 -contribution of

$$\chi^2 = \frac{f_{\text{sky}}}{\pi} \frac{1}{(2\pi)^2} \int d^2 \ell_{1,2,3} d^2 \ell_{1',2',3'} \delta_{\text{D}}(\ell_1 + \ell_2 + \ell_3) B_{i_1 i_2 i_3}^{\ell_1, \ell_2, \ell_3} \text{Cov}^{-1} \left[\tilde{B}_{i_1 i_2 i_3}^{\ell_1, \ell_2, \ell_3}, \tilde{B}_{i_1' i_2' i_3'}^{\ell_1', \ell_2', \ell_3'} \right] \tilde{B}_{i_1' i_2' i_3'}^{\ell_1', \ell_2', \ell_3'}, \quad (\text{A1})$$

where also the sum over all field indices is implied. However, the integrand is symmetric in any simultaneous pairwise permutation of (ℓ_n, i_n) with (ℓ_m, i_m) and likewise of (ℓ'_n, i'_n) with (ℓ'_m, i'_m) . This type of redundancy can be avoided by constraining the integration volumes to $\ell_1 < \ell_2 < \ell_3$ and $\ell'_1 < \ell'_2 < \ell'_3$. Furthermore, the sum over field indices may lead to more redundancy, which we encode at this point into a multiplicity factor $s_{i_1 i_2 i_3}^{i_1' i_2' i_3'}$. Now, the signal-to-noise ratio can be written as

$$\begin{aligned} (\Sigma^{(3)})^2 &= \frac{f_{\text{sky}}}{4\pi^3} \int_{\ell_1 < \ell_2 < \ell_3} d^2 \ell_{1,2,3} \int_{\ell'_1 < \ell'_2 < \ell'_3} d^2 \ell_{1',2',3'} \delta_{\text{D}}(\ell_1 + \ell_2 + \ell_3) \\ &\times B_{i_1 i_2 i_3}^{\ell_1, \ell_2, \ell_3} \text{Cov}^{-1} \left[\tilde{B}_{i_1 i_2 i_3}^{\ell_1, \ell_2, \ell_3}, \tilde{B}_{i_1' i_2' i_3'}^{\ell_1', \ell_2', \ell_3'} \right] \tilde{B}_{i_1' i_2' i_3'}^{\ell_1', \ell_2', \ell_3'} \left(s_{i_1 i_2 i_3}^{i_1' i_2' i_3'} \right)^{-1}, \quad (\text{A2}) \end{aligned}$$

In this subspace the covariance matrix can be inverted, as it was shown in Section 4.2. Substituting eqn. (47) into eqn. (A2), we find

$$\begin{aligned} (\Sigma^{(3)})^2 &= \frac{f_{\text{sky}}}{4\pi^3} \left(s_{i_1 i_2 i_3}^{i_1' i_2' i_3'} \right)^{-1} \int_{\ell_1 < \ell_2 < \ell_3} d^2 \ell_1 d^2 \ell_2 \\ &\times B_{i_1 i_2 i_3}^{\ell_1, \ell_2, \ell_3} \frac{\tilde{C}_{i_1' i_1'}^{\ell_1} \tilde{C}_{i_2' i_2'}^{\ell_2} \tilde{C}_{i_3' i_3'}^{\ell_3}}{\det C^{\ell_1} \det C^{\ell_2} \det C^{\ell_3}} \tilde{B}_{i_1' i_2' i_3'}^{\ell_1, \ell_2, \ell_3}, \quad (\text{A3}) \end{aligned}$$

where from now on $\ell_3 = -\ell_1 - \ell_2$ is implied, if ℓ_3 is not integrated over. If one is now interested in the signal-to-noise ratio of particular field mixture, i.e. data with a fixed field configuration $q = i_1 + i_2 + i_3$, one can further simplify the expression. For pure galaxy contributions, $q = q' = 0$, we can neglect the cross-correlation, i.e. $C_{01} = 0$, and no redundancy due to field summation occurs, $s_{000}^{000} = 1$. One obtains the well-known case (Hu 2001)

$$(\Sigma_0^{(3)})^2 = \frac{f_{\text{sky}}}{4\pi^3} \int d^2 \ell_1 d^2 \ell_2 \frac{\left(B_{000}^{\ell_1, \ell_2, \ell_3} \right)^2}{6 \tilde{C}_{00}^{\ell_1} \tilde{C}_{00}^{\ell_2} \tilde{C}_{00}^{\ell_3}}, \quad (\text{A4})$$

where the symmetry in the integrand was used to obtain an integration over full ℓ -space in combination with the factor 1/6. If all mixed spectra with one iSW field are taken into account, i.e. $q = q' = 1$, one obtains 9 different contributions due to the field index summation. Three contributions are quadratic in identical bispectra, $(i_1, i_2, i_3) = (i_1', i_2', i_3')$, and have multiplicity one. The remaining mixed contributions have multiplicity 2, since the integrand in eqn. (A3) is symmetric under exchange of the primed and unprimed index sets (i_1, i_2, i_3) and (i_1', i_2', i_3') as a whole. Therefore the multiplicities are

$$\begin{aligned} 1 &= s_{001}^{001} = s_{010}^{010} = s_{100}^{100} \\ 2 &= s_{001}^{010} = s_{001}^{100} = s_{010}^{100} = s_{010}^{001} = s_{100}^{001} = s_{100}^{010}. \quad (\text{A5}) \end{aligned}$$

If one uses

$$\begin{aligned} B_{010}^{\ell_1, \ell_2, \ell_3} &= B_{001}^{\ell_1, \ell_3, \ell_2} \\ B_{100}^{\ell_1, \ell_2, \ell_3} &= B_{001}^{\ell_3, \ell_2, \ell_1} \end{aligned} \quad (\text{A6})$$

in combination with

$$B_{001}^{\ell_1, \ell_2, \ell_3} = \frac{1}{2} \left(B_{001}^{\ell_1, \ell_2, \ell_3} + B_{001}^{\ell_2, \ell_1, \ell_3} \right), \quad (\text{A7})$$

one can combine the quadratic terms to one, which is integrated over the full $\ell_{1,2,3}$ -volume. This can be done for the mixed terms in analogy and one is left with the following expression for the signal-to-noise ratio,

$$\begin{aligned} (\Sigma_1^{(3)})^2 &= \frac{f_{\text{sky}}}{4\pi^3} \int d^2 \ell_1 d^2 \ell_2 \left(2 \det C^{\ell_1} \det C^{\ell_2} \det C^{\ell_3} \right)^{-1} \\ &\left[\left(B_{001}^{\ell_1, \ell_2, \ell_3} \right)^2 \tilde{C}_{11}^{\ell_1} \tilde{C}_{11}^{\ell_2} \tilde{C}_{00}^{\ell_3} + B_{001}^{\ell_1, \ell_2, \ell_3} \tilde{C}_{11}^{\ell_1} \tilde{C}_{01}^{\ell_2} \tilde{C}_{01}^{\ell_3} B_{010}^{\ell_1, \ell_2, \ell_3} \right]. \quad (\text{A8}) \end{aligned}$$

Following the analog path of argumentation one finds the signal-to-noise expressions for the trispectra to be

$$\begin{aligned} (\Sigma_0^{(4)})^2 &= \frac{f_{\text{sky}}}{8\pi^4} \int d^2 \ell_1 d^2 \ell_2 d^2 \ell_3 \frac{\left(T_{0000}^{\ell_1, \ell_2, \ell_3, \ell_4} \right)^2}{24 \tilde{C}_{00}^{\ell_1} \tilde{C}_{00}^{\ell_2} \tilde{C}_{00}^{\ell_3} \tilde{C}_{00}^{\ell_4}} \\ (\Sigma_1^{(4)})^2 &= \frac{f_{\text{sky}}}{8\pi^4} \int d^2 \ell_1 d^2 \ell_2 d^2 \ell_3 \left(\det C^{\ell_1} \dots \det C^{\ell_4} \right)^{-1} \\ &\left[\frac{1}{6} \left(T_{0001}^{\ell_1, \ell_2, \ell_3, \ell_4} \right)^2 \tilde{C}_{11}^{\ell_1} \tilde{C}_{11}^{\ell_2} \tilde{C}_{11}^{\ell_3} \tilde{C}_{00}^{\ell_4} \right. \\ &\left. + \frac{1}{4} T_{0001}^{\ell_1, \ell_2, \ell_3, \ell_4} \tilde{C}_{11}^{\ell_1} \tilde{C}_{11}^{\ell_2} \tilde{C}_{01}^{\ell_3} \tilde{C}_{01}^{\ell_4} T_{0010}^{\ell_1, \ell_2, \ell_3, \ell_4} \right]. \quad (\text{A9}) \end{aligned}$$

Also the expressions for higher values of q can now be deduced with the same techniques.

This paper has been typeset from a $\text{\TeX}/\text{\LaTeX}$ file prepared by the author.